# Examining the Connection Between PAH and MIR Emission Features and Physical Processes in Ultra Luminous Infrared Galaxies

Lauren Robinson[a,b], Duncan Farrah[a,c]

[a]*Institute for Astronomy, University of Hawai'i, 2680 Woodlawn Drive, Honolulu, HI 96822, USA*

[b]*Department of Physics and Astronomy, Ohio State University, 281 West Lane Avenue, Columbus, OH 43210, USA*

[c]*Department of Physics and Astronomy, University of Hawai'i, 2505 Correa Road, Honolulu, HI 96822, USA*

**Abstract**

We examine the relationship between Polycyclic Aromatic Hydrocarbon features, and physical characteristics for a sample of 42 ULIRGs observed using the Infrared Spectrograph on the *Spitzer Space Telescope*. A radiative transfer model has decomposed the total infrared luminosity into component luminosities: starburst, spheroid, and AGN luminosity. We run kendall tau correlation tests to determine if there is a correlation between PAH features and the physical processes that occur throughout these ULIRGs. We then develop linear models of the data in log space. We observe strong correlations between PAH Luminosities and starburst luminosity, supporting the theory that PAH emission features are the result of gas in the ISM being heated by photons from stars. Furthermore, we find a correlation between PAH luminosity and star formation rate, meaning that PAH molecules are being heated by young, newly formed stars. We find a significant anti-correlation between PAH EW and AGN luminosity. We explore how these relationships change with respect to a third variable, including properties of the starburst, properties of the AGN, and silicate depth.

*Keywords:* Infrared, Galaxies, Starburst, Active Galactic Nuclei, Polycylcic Aromatic Hydrocarbon, Ultra Luminous Infrared Galaxies

## 1. Introduction

Ultra Luminous Infrared Galaxies, ULIRGs, are Galaxies with Infrared (IR; 780 nm - 1000 $\mu m$) luminosities above $10^{12} L_{\odot}$, ($L_{\odot} \approx 3.827 \cdot 10^{26}$ Watts) (Lonsdale et al., 2006). The

*Email address:* Robinson.2407@buckeyemail.osu.edu (Lauren Robinson)

Infrared Astronomical Satellite was the first satellite to discover a significant number of ULIRGs in 1983 (Lonsdale et al., 2006). ULIRGs are sparse within $z < 0.3$, having a density on the sky of less than one per one hundred square degrees (Soifer and Neugebauer, 1991; Lonsdale et al., 2006; Vaccari et al., 2010). However, the density of ULIRGs increases towards higher redshift, reaching several hundred per square degree for $z \geq 1$ (Rowan-Robinson et al., 1997; Dole et al., 2001; Borys et al., 2003; Mortier et al., 2005; Austermann et al., 2010; Goto et al., 2011; Farrah et al., 2013). The power source behind the IR emission of these galaxies is believed to be a combination of starbursts and Active Galactic Nuclei (AGN) activity. The bulk of stellar and black hole mass assembly occurs at high redshift, with roughly half of observed stellar mass being formed before z = 1.3, where ULIRGs are more prominent (Madau and Dickinson, 2014). Therefore, understanding the formation process of ULIRGs is crucial to understanding the formation process of galaxies as a whole.

Examining fine structure lines and emission features of local ULIRGs can provide insight to the star formation rate (SFR), rapid black hole mass accretion (AGN), and other physical processes within galaxies. Our understanding of the relationship between emission features and observable physical processes in infrared galaxies is limited. Observing at high redshift is quite difficult, as the objects being observed are incredibly far away, making them difficult to resolve and appearing dimmer. Additionally, the majority of ULIRG activity is obscured by dust and gas in the interstellar medium. For these reasons, we examine local ULIRGs (because they are accessible) in the mid-infrared (minimizing the obscurity).

We are particularly interested in the relationship between starbursts and Polycyclic Aromatic Hydrocarbon (PAH) emission features. Starbursts are regions which have a high star formation rate. Ultra Violet (UV) and optical photons radiate off of the many stars in these formation regions, heating PAH molecules in the surrounding ISM. The atoms in these molecules become excited, causing them to vibrate and radiate infrared emissions which have been detected by the Spitzer space telescope. Emission features for PAHs, ($6.2\mu m$ and $11.1\mu m$), have been collected for 42 local ULIRGs using the *Spitzer* Infrared Spectrograph.

In this paper, we explore the relationship between PAH emission features and star formation rate, AGN accretion rate, and other characteristics of ULIRGs, using the results of a radiative transfer model. This model has separated the IR luminosity of ULIRGs into three components: starburst, spheroid, and AGN luminosity. We aim to develop a scaling relationship between components of IR luminosity and observed MIR features in local ULIRGs. Additionally, we analyze the effects of a third variable,including properties of starburst (starburst age $Age_{SB}$, initial optical depth of star formation $\tau_V$, and the time constant of the exponentially decaying SFR $\tau_{SB}$), AGN (inclination angle $\theta_{inc}$, opening angle $\theta_o$, and UV optical depth, $\tau_{UV}$), and silicate depth $\tau_{Si}$ on the scaling relationships developed.

## 2. Method

### *2.1. The Data*

The sample was obtained using the Infrared Spectrograph on the *Spitzer* space telescope as part of the garaunteed time observations program. The flux limited sample is composed of 42 ULIRGs with flux densities $\geq 2Jy$ and z $< 0.23$. More detailed information about the sample can be found in Farrah et al. (2013), and information on the observations can be found in Desai et al. (2007). Only 39 of these galaxies had data for 6.2 PAH luminosity and only 40 had data for 11 PAH luminosity, so all tests run and models created involving PAH emissions used either 39 or 40 ULIRGs respectively.

### *2.2. Radiative Transfer Model*

Using a radiative transfer model, we are able to decompose the IR luminosity into several components: AGN, spheroid (host galaxy), and starburst luminosity. This allows us to test for correlations and develop scaling relations between PAH emission and component luminosities. This model also corrects the luminosities of the AGN in the ULIRGs to account for anisotropic emission of the torus. We examine both "raw" (data that has not been corrected), and corrected data. For more information on the radiative transfer model refer to Efstathiou et al. (2022).

### *2.3. Kendall Rank Correlation Coefficient*

Using SciPy statistics, we found the Kendall Rank Corellation Coefficient, Kendall's Tau between all pairs of emission features and observable physical processes. Kendall's Tau is a correlation coefficient used to quantify the strength of the relationship between two sets of data. This test is optimal in that it does not assume any sort of model, and looks for a correlation in any form. The value ranges from -1 to 1. -1 corresponding to a strong anti-correlation, 0 corresponding to a lack of correlation, and 1 corresponding to a strong positive correlation. Additionally, SciPy statistics returns a P-value for all correlation tests. Generally, the null hypothesis can be rejected when a P-value of $P < .05$ is obtained. The null hypothesis in this paper is that there is *no* relationship between PAH emission features and observables in ULIRGs.

We first use Kendall's tau correlation tests to determine the probability of a correlation between emission features and component luminosity. If a statistically significant (P $\leq$ 0.05) correlation is found, we further explore the relationship by creating a model.

### *2.4. Developing a Model*

The initial analysis of Mid-infrared fine structure line luminosities and physical properties of ULIRGs consists of fitting the data to a linear model in log space. Model's take the form

$$log(L_{Component}) = \alpha \cdot log(L_{Observable}) + \beta \quad (1)$$

The models were created using the SciPy package Orthogonal Distance Regression (ODR). ODR minimizes the sum of perpendicular (orthogonal) distances squared, and outputs a slope and intercept of a linear model with consideration of errors in both $L_{Component}$ and $L_{Observable}$.

## 3. Results and Discussion

### *3.1. 6.2 and 11 μm PAH Emission*

#### *3.1.1. Deriving Relationships*

We begin our analysis by running Kendall tau correlation tests for PAH luminosities against all component luminosities. After establishing whether or not a correlation exists, we perform parameter fits.

In the sample, significant correlations have been found between starburst luminosity and 6.2 and 11 $\mu$m PAH luminosities. This is consistent with the theory that PAH emissions are the result of molecular gas being heated by starlight. Between 6.2 $\mu$m PAH emission and starburst luminosity $L_{Sb}$, we find Kendall's correlation coefficient and P-value to be $\tau = 0.52$ and $P = 3.60 \cdot 10^{-6}$ respectively. The scaling relationship between 6.2 $\mu$m PAH emission and starburst luminosity is

$$log(L_{Sb}) = (0.724 \pm 0.114) \cdot log(L_{6.2\mu m}) + (5.425 \pm 1.050)$$

Between 11 $\mu$m PAH emission and $L_{Sb}$, we find $\tau = 0.56$ and $P = 3.34 \cdot 10^{-7}$. The scaling relationship between 11 $\mu$m PAH emission and starburst luminosity is

$$log(L_{Sb}) = (0.785 \pm 0.111) \cdot log(L_{11\mu m}) + (4.949 \pm 1.007)$$

Ideally with no interference from other processes, the slope of both of these relationships would be on the order of unity. The 6.2 $\mu$m slope is consistent with unity for $\pm 3\sigma$ and the 11 $\mu$m relation slope is consistent with unity for $\pm 2\sigma$. The scaling relationships are consistent with one another to $\pm 1\sigma$. It is interesting to note that while the relationships are consistent with unity, the slopes fall outside of unity by more than $1\sigma$. There are roughly 4 possible reasons for why this is the case. First, it is possible that there only exist a set number of PAH molecules, and therefore emission features approach a maximum. Second, it is also possible that some fraction of the emissions come from a source other than starbursts. Third, it may be that an increase of stars, meaning an increase in super nova, leads to an increase in the amount of dust and therefore the PAH emissions are more heavily obscured for galaxies with larger starbursts. Fourth, it may also be that stars above a certain luminosity begin to destroy PAH molecules.

We believe the most plausible explanation is that stars above a certain luminosity begin to destroy PAH molecules. The other explanations are less possible. If PAH emissions

approached some maximum, we would have derived a steeper slope, rather than a shallower one. If there existed another source of luminosity that produced PAH features, this source would need to produce PAH emissions on roughly the same scale as starbursts. We find no correlation between AGN luminosity, and while a correlation between PAH luminosity and spheroid luminosity is present, the spheroid luminosity is roughly an order of magnitude lower than the starburst luminosity. Thus, it is not likely that the spheroid luminosity could be responsible for a significant fraction of PAH emissions. Additionally, if PAH emissions came from the host galaxy, we would see a weaker correlation between $L_{Sb}$ and $L_{PAH}$ for galaxies with lower $L_{sb}/L_{Sph}$ ratios. We find no significant difference in the strength of the correlation, or the slope of the scaling relation between galaxies with high and low $L_{sb}/L_{Sph}$ ratios.

If starbursts above a certain luminosity destroyed PAH molecules, we would notice a flattening of correlation for galaxies with the highest starburst luminosities. After dividing the sample into those with $L_{SB}$ above and below the mean $L_{SB}$, we find a significant correlation between starburst luminosity and PAH emissions for galaxies with lower starburst luminosities only. This may be a result of the small sample size. The models developed between $L_{SB}$ and PAH luminositiy for galaxies with lower $L_{SB}$ have shallower slopes than the original models derived above, but are consistent to $\pm 3\sigma$.

If PAH emissions are more heavily obscured in galaxies with more luminous starbursts, we would expect to see a change in correlation for galaxies with higher initial optical depth of the starburst. When we divide the sample by optical depth and run correlation tests, we get a higher $\tau$ and lower P-value for galaxies with higher optical depth. However, we find no significant difference in the models derived for galaxies with lower and higher optical depth.

Next, we examine the relationship between PAH luminosity and SFR. Significant correlations have been found between SFR and 6.2 and 11 $\mu$m PAH luminosities. Between 6.2 $\mu$m PAH emission and SFR, we find $\tau = 0.55$ and $P = 7.51 \cdot 10^{-7}$. The scaling relationship between 6.2 $\mu$m PAH emission and SFR is

$$log(SFR) = (0.875 \pm 0.124) \cdot log(L_{6.2\mu m}) + (-5.519 \pm 1.147)$$

Between 11 $\mu$m PAH emission and SFR, we find $\tau = 0.56$ and $P = 3.78 \cdot 10^{-7}$. The scaling relationship between 11 $\mu$m PAH emission and SFR is

$$log(SFR) = (0.880 \pm 0.133) \cdot log(L_{11\mu m}) + (-5.467 \pm 1.205)$$

We find evidence of a positive correlation between star formation rate and the relationships developed above. That is, galaxies with higher star formation rates appear to have greater PAH emission and starburst luminosity. We note that our derived relationships between PAH luminosity and SFR have slightly larger slopes, but they are consistent with the $L_{Sb}$ relations to $\pm 2\sigma$ for 6.2 $\mu$m and $\pm 1\sigma$ for 11 $\mu m$. We also note that the SFR relations have greater residual variances (0.58 and 0.71 for 6.2 and 11 $\mu$m respectively) compared to $L_{SB}$ relations (0.36 and 0.37 respectively).

We examine how the relationship between starburst luminosity and PAH luminosity varies

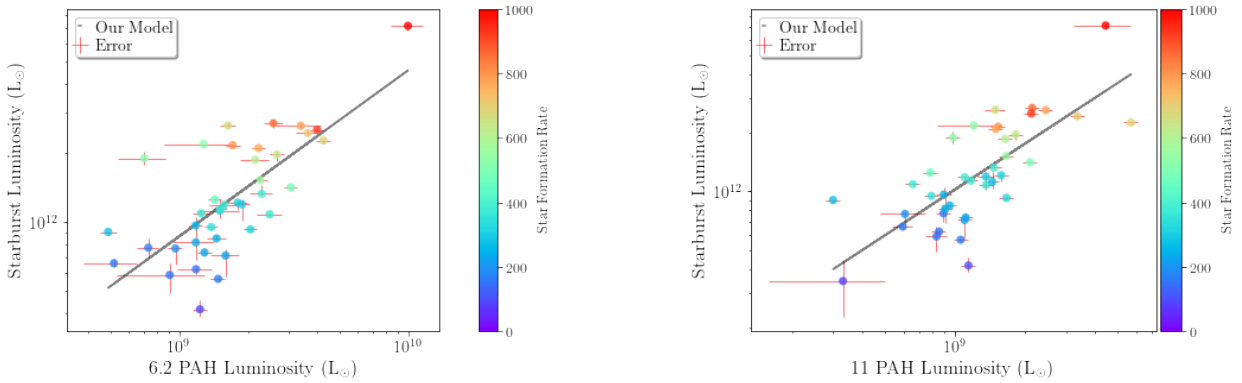


Figure 1: Starburst luminosity versus 6.2 $\mu$m (left) and 11 $\mu$m (right) PAH luminosity, color coded by star formation rate. Models derived above are plotted atop of the data

with respect to a third variable. We first determine if relations depend on properties of starbursts, such as starburst age, initial optical depth, and star formation rate e-folding time. No significant differences were found in the correlation between both 6.2 and 11 $\mu$m PAH luminosity and starburst luminosity with respect to properties of the starburst.

We then explore if the relationship is dependant on properties of AGN, such as UV optical depth, inclination angle, and opening angle. No significant differences were found in the correlation between both 6.2 and 11 $\mu$m PAH luminosity and starburst luminosity with respect to properties of the AGN.

Next, we explore the relationship with respect to silicate depth. No significant differences were found in the correlation between both 6.2 and 11 $\mu$m PAH luminosity and starburst luminosity with respect to silicate depth.

We then examine the relationship between PAH luminosity and spheroid luminosity. We find significant correlations between spheroid luminosity and PAH luminosity. Between 6.2 $\mu$m PAH emission and $L_{Sph}$, we find $\tau = 0.247$ and $P = 0.027$. The scaling relationship between 6.2 $\mu$m PAH emission and spheroid luminosity is

$$log(L_{sph}) = (0.860 \pm 0.249) \cdot log(L_{6.2\mu m}) + (2.901 \pm 2.299)$$

Between 11 $\mu$m PAH emission and $L_{Sb}$, we find $\tau = 0.223$ and $P = 0.043$. The scaling relationship between 11 $\mu$m PAH emission and spheroid luminosity is

$$log(L_{sph}) = (0.860 \pm 0.284) \cdot log(L_{11\mu m}) + (3.028 \pm 2.585)$$

While a correlation between spheroid luminosity and PAH luminosity is detected, we do not believe that a significant portion of PAH emission features come from the host galaxy. We find no significant difference in the strength of the correlation, or the slope of the scaling relation shown above between galaxies with high and low $L_{sb}/L_{Sph}$ ratios. If PAH emissions came from the host galaxy, we would see a stronger correlation between $L_{Sph}$ and $L_{PAH}$ for galaxies with lower $L_{sb}/L_{Sph}$ ratios. We therefore conclude that the host galaxy does not

make a significant contribution to PAH emissions.

We explore how the relationship between PAH luminosity and spheroid luminosity varies with respect to properties of the starburst, AGN, and silicate depth. We find no dependence on third variables.

We then examine the relationship between PAH luminosity and AGN luminosity. We test for correlations between both raw and corrected AGN luminosity. We find no significant correlation between raw or corrected AGN luminosity and PAH luminosity.

We examine the relationship between PAH luminosity and total luminosity. We test for correlations between both raw and corrected total luminosity. Significant correlations have been found between raw total luminosity and 6.2 and 11 $\mu$m PAH luminosities. This is expected, as starburst luminosity makes up a portion of the total luminosity. Between 6.2 $\mu$m PAH emission and $L^r_{tot}$, we find $\tau = 0.41$ and $P = 0.0002$. The scaling relationship between 6.2 $\mu$m PAH emission and raw total luminosity is

$$log(L^r_{tot}) = (0.553 \pm 0.119) \cdot log(L_{6.2\mu m}) + (7.158 \pm 1.098)$$

Between 11 $\mu$m PAH emission and $L^r_{tot}$, we find $\tau = 0.45$ and $P = 4.11 \cdot 10^{-5}$. The scaling relationship between 11 $\mu$m PAH emission and raw total luminosity is

$$log(L^r_{tot}) = (0.550 \pm 0.117) \cdot log(L_{11\mu m}) + (7.254 \pm 1.062)$$

However, there were no statistically significant correlations found for corrected total luminosity. This is a reasonable result, seeing as there is no correlation observed between AGN luminosity and PAH luminosity. The corrected total luminosity includes corrected AGN luminosity, which is generally greater than the raw AGN luminosity. So, when a larger portion of the total luminosity is made up of AGN luminosity, the correlation observed between PAH luminosity and starburst and spheroid luminosity is hidden. For an explanation as to why the corrected AGN luminosities are systematically greater than the raw luminosities, refer to Efstathiou et al. (2022).

We explore how the relationship between PAH luminosity and total luminosity varies with respect to properties of the starburst, AGN, and silicate depth. We find a correlation between total luminosity and SFR (also likley due to the starburst component). We find no dependence on other properties of starburst, properties of AGN, or silicate depth.

### *3.1.2. Comparison to Literature*

After developing some basic scaling relationships, we compare our results to other literature. Papers such as Cortzen et al. (2019) developed scaling relations between the infrared luminosity and 6.2 PAH luminosity for star forming galaxies (SFGs). Cortzen used a sample of 34 "star-forming targets" from the 5 mJy Unbiased Spitzer Extragalactic Survey (5MUSES) with redshift $0.03 < z < 0.28$ and $L_{IR} \approx 10^{10}L_\odot - 10^{12}L_\odot$ (Cortzen et al., 2019). They developed equations of the form $log(L_{6.2\mu m}) = \alpha \cdot log(L_{IR}) + \beta$. For star forming galaxies they found $\alpha = 0.98 \pm 0.03$ and $\beta = -1.89 \pm 0.30$. We attempt to replicate this relationship by creating a scaling relationship between PAH luminosity and the sum of starburst and

host galaxy luminosity.

We find correlations between the sum of spheroid and starburst luminosity and PAH luminosity. Between 6.2 $\mu$m PAH emission and $L_{Sb+Sph}$, we find $\tau = 0.59$ and $P = 3.92 \cdot 10^{-8}$. The scaling relationship between 6.2 $\mu$m PAH emission and $L_{Sb+Sph}$ is

$$log(L_{6.2\mu m}) = (1.366 \pm 0.152) \cdot log(L_{sph+sb}) + (-7.373 \pm 1.836)$$

For completeness we derive the same relation for 11 $\mu$m PAH Emissions. Between 11 $\mu$m PAH emission and $L_{Sb+Sph}$, we find $\tau = 0.61$ and $P = 1.12 \cdot 10^{-8}$. The scaling relationship between 11 $\mu$m PAH emission and $L_{Sb+Sph}$ is

$$log(L_{11\mu m}) = (1.379 \pm 0.197) \cdot log(L_{sph+sb}) + (-7.641 \pm 2.386)$$

Both the slope and intercept of our 6.2 $\mu$m model are consistent with the scaling relation for SFGs in Cortzen et al. (2019) to $\pm 3\sigma$.

Cortzen et al. (2019) also developed a scaling relation between infrared luminosity and 6.2 PAH luminosity for all galaxies in their sample, rather than exclusively SFGs. For *all* galaxies they found $\alpha = 0.81 \pm 0.03$ and $\beta = -0.04 \pm 0.29$. Our $\alpha$ is consistent with the relationship derived by Cortzen et al. (2019) for all galaxies for $\pm 3\sigma$. Our $\beta$ is not consistent with said relationship.

We found no significant correlation between PAH luminosity and total corrected luminosity in our sample, and thus chose not to derive a scaling relation. We derive a scaling relation for 6.2 PAH emission as a function of raw total luminosity, and obtain a result consistent with the scaling relation for all galaxies derived in Cortzen et al. (2019). We have plotted both of the models presented in Cortzen et al. (2019) along with our own model atop of the data below.

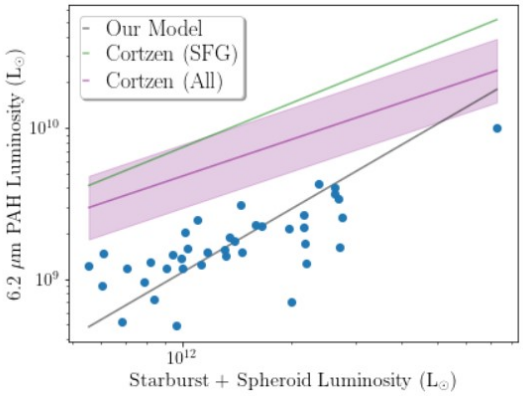


Figure 2: 6.2 $\mu$m PAH Luminosity versus $L_{Sb} + L_{Sph}$, including both models developed by Cortzen et al. (2019) and our own model. Cortzen's full sample model is shaded for $\pm 1\sigma$.

The stark difference in the models versus the data may be due to one of several different reasons. Cortzen's models predict a higher PAH luminosity than our galaxies have for the observed $L_{Sb} + L_{Sph}$. Cortzen noted that ULIRGs lie over 3 $\sigma$ from the best-fitting relations. Our sample of ULIRGs similarly lies between 1-4 $\sigma$ from the model developed using Cortzen's

full sample. There are several possible explanations for this. There may be PAH detection interference, an additional source of luminosity, or PAH emission interference. Cortzen suggests that the lower $L_{PAH}/L_{IR}$ ratios observed in AGN dominated sources (compared to SFGs) may be the result of 6.2, 7.7, and 8.6 $\mu$m PAH emissions being suppressed by the AGN. We believe that this suppression is due to detection interference. We explore this further in section 3.2, when we develop models between PAH EW and $L_{AGN}$.

Other texts have developed scaling relationships between PAH luminosity and star formation rate. For instance, Maragkoudakis et al. (2018) developed a star formation rate to PAH luminosity relationship for galaxies M83 and M33 using Spitzer spectra for 21 and 18 HII regions respectively. The results are as follows

$SFR(M_{\odot}yr^{-1}) = 9.72 \cdot 10^{-31} \cdot [L_{PAH6.2}(ergs^{-1})]^{0.7}$ for $L_{6.2\mu m}$ and

$SFR(M_{\odot}yr^{-1}) = 1.09 \cdot 10^{-31} \cdot [L_{PAH11.3}(ergs^{-1})]^{0.72}$ for $L_{11\mu m}$

We take the logarithm of these equations in order to compare them to models we have created ourselves

$log(SFR(M_{\odot}yr^{-1}) = 0.7 \cdot log(L_{PAH6.2}(ergs^{-1})) - 30.012$ for $L_{6.2\mu m}$ and

$log(SFR(M_{\odot}yr^{-1}) = 0.72 \cdot log(L_{PAH11.3}(ergs^{-1})) - 30.963$ for $L_{11\mu m}$

We re-derive the relationship between SFR and PAH emission, now with PAH luminosity in $ergs^{-1}$. We find that for both 6.2 and 11 PAH luminosity, our slopes are consistent with Maragkoudakis et al. (2018) for $\pm 2\sigma$ and our intercepts are consistent to $\pm 1\sigma$.

Shipley et al. (2016) also developed linear scaling relations between PAH emissions and SFR using IRS/Spitzer observations of a sample of 105 galaxies with IR luminosities between $10^9 - 10^{12} L_{\odot}$. SFR were derived using extinction-corrected $H_{\alpha}$. Their results are as follows:

$log(SFR(M_{\odot}yr^{-1}) = (0.96 \pm 0.04) \cdot log(L_{PAH6.2}(ergs^{-1})) + (-40.06 \pm 0.09)$ for $L_{6.2\mu m}$ and

$log(SFR(M_{\odot}yr^{-1}) = (1.06 \pm 0.03) \cdot log(L_{PAH11.3}(ergs^{-1})) + (-44.14 \pm 0.08)$ for $L_{11\mu m}$

Our results for $6.2\mu m$ are consistent with Shipley et al. (2016) to $\pm 1\sigma$, and our $11\mu m$ relation is consistent to $\pm 2\sigma$.

Our model, along with those from Shipley et al. (2016) and Maragkoudakis et al. (2018) are plotted atop of the data in figure 3. The difference in the models is reasonable given the differences in our respective samples. Maragkousdakis had a small sample size of 2 galaxies, both of which were much less luminous than the ULIRGs in our sample, and half of Shipley's sources were over an order of magnitude less luminous than those in our own sample.

### *3.2. Equivalent Width*

We continue our analysis by running Kendall tau correlation tests for PAH Equivalent Width (EW) against all component luminosities. After establishing whether or not a correlation exists, we perform parameter fits.

Notably, we find no correlation between PAH EW and starburst luminosity or spheroid

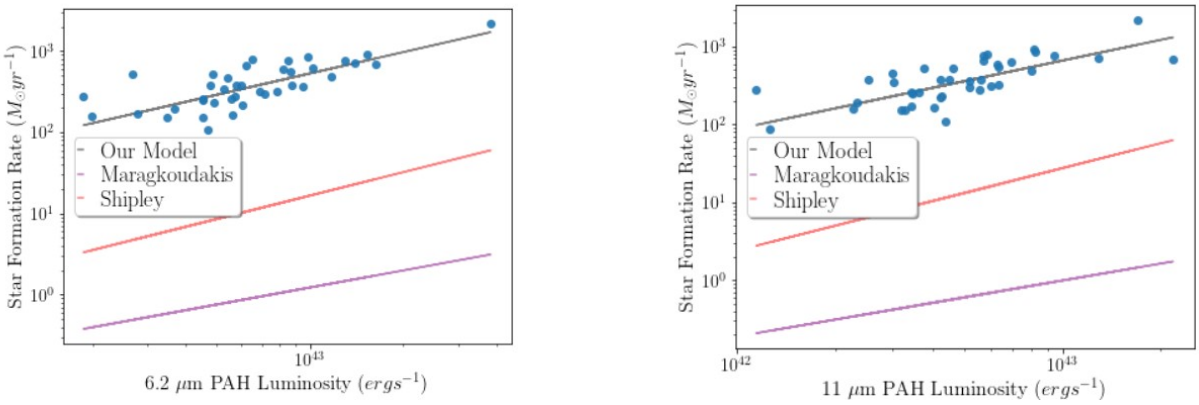


Figure 3: Star formation rate versus both 6.2 and 11 $\mu$m PAH luminosity. Models derived by Maragkoudakis et al. (2018) (purple) and Shipley et al. (2016) (red) are plotted atop of the data, along with our own model (black).

luminosity, both of which had an observed correlation with PAH luminosity. PAH EW measures emission features relative to the continuum. So, while galaxies with higher $L_{Sb}$ and $L_{Sph}$ have greater PAH luminosity, the PAH luminosity is not necessarily bright relative to the continuum. These results may be due to an additional continuum source. Infact, starbursts may produce continuum proportional to the PAH emissions produced.

If starbursts produced continuum proportional to PAH emissions, then we would not expect to find evidence of a correlation between PAH EW and raw AGN luminosity. We find significant anti-correlation between PAH EW and raw AGN luminosity, supporting the theory that AGN destroy or interfere with our ability to observe PAH emission features.

Between 6.2 $\mu$m PAH EW and $L^r_{AGN}$, we find $\tau = -0.46$ and $P = 3.707 \cdot 10^{-7}$. The scaling relationship between 6.2 $\mu$m PAH EW and raw AGN luminosity is

$$log(L^r_{AGN}) = (-0.609 \pm 0.099) \cdot log(6.2 \mu m EW) + (11.023 \pm 0.088)$$

Between 11 $\mu$m PAH EW and $L^r_{AGN}$, we find $\tau = -0.333$ and $P = 0.002$. The scaling relationship between 11 $\mu$m PAH EW and raw AGN luminosity is

$$log(L^r_{AGN}) = (-0.525 \pm 0.111) \cdot log(11 \mu m EW) + (11.198 \pm 0.082)$$

We believe the most likely explanation for these results is that bright AGN are cause for a bright continuum, making it difficult to observe PAH emissions on said continuum. Another explanation for this result is that galaxies with greater AGN luminosity have lower starburst luminosities, and therefore less PAH emissions. If this were the case, we would also observe an anti-correlation between $L^r_{AGN}$ and $L_{Sb}$, which we do not find.

Next, we examine the correlation between PAH EW and corrected AGN luminosity. We find a significant anti-correlation between 6.2 $\mu$m EW and $L^c_{AGN}$, but no significant correlation or anti-correlation between $L^c_{AGN}$ and 11 $\mu$m EW.

Between 6.2 $\mu$m PAH EW and $L^c_{AGN}$, we find $\tau = 0.233$ and $P = 0.036$. The scaling relationship between 6.2 $\mu$m PAH EW and corrected AGN luminosity is

$$log(L^c_{AGN}) = (-0.556 \pm 0.182) \cdot log(L_{6.2\mu m}) + (11.620 \pm 0.158)$$

No significant differences were found in the correlation between both 6.2 and 11 $\mu$m PAH EW and AGN luminosity with respect to properties of the starburst, AGN, or with respect to silicate depth.

## 4. Conclusions

We present linear models between 6.2 and 11 $\mu$m PAH emissions and SFR as well as starburst, spheroid, AGN, and total luminosity of our sample of 42 galaxies. These models are best used to convert between PAH luminosity and component luminosities in very luminous systems. We confirm that PAH emissions are the result of star formation. These emission features are harder to detect when a strong continuum is present, and AGN are a source of this continuum. In particular we find positive correlations between PAH emissions, starburst, spheroid, and total luminosity, as well as SFR. We find negative correlations between PAH EW and AGN luminosity. We explore the dependence of these emission lines and relationships with respect to properties of the starburst, AGN, and silicate depth and find no significant influence from these variables. We compare our results to those in other texts and find reasonable differences due to differences between our samples. The next step will be to explore the relationship between the mid infrared fine structure lines and component luminosities, develop scaling relationships (if evidence of a correlation exists) and analyze said relationships.

## Acknowledgements

LR acknowledges support from Research Experience for Undergraduate program at the Institute for Astronomy, University of Hawaii-Manoa funded through NSF grant #2050710. LR would like to thank the Institute for Astronomy for their hospitality during the course of this project.

Software: matplotlib (Hunter, 2007), numpy (Harris et al., 2020), Scipy (Jones et al., 2001–), pandas (Wes McKinney, 2010).

## References


J. E. Austermann, J. S. Dunlop, T. A. Perera, K. S. Scott, G. W. Wilson, I. Aretxaga, D. H. Hughes, O. Almaini, E. L. Chapin, S. C. Chapman, M. Cirasuolo, D. L. Clements, K. E. K. Coppin, L. Dunne, S. Dye, S. A. Eales, E. Egami, D. Farrah, D. Ferrusca, S. Flynn, D. Haig, M. Halpern, E. Ibar, R. J. Ivison, E. van Kampen, Y. Kang, S. Kim, C. Lacey, J. D. Lowenthal, P. D. Mauskopf, R. J. McLure, A. M. J. Mortier, M. Negrello, S. Oliver, J. A. Peacock, A. Pope, S. Rawlings, G. Rieke, I. Roseboom, M. Rowan-Robinson, D. Scott, S. Serjeant, I. Smail, A. M. Swinbank, J. A. Stevens, M. Velazquez, J. Wagg, and M. S. Yun. AzTEC half square degree survey of the SHADES fields - I. Maps, catalogues and source counts. MNRAS, 401(1):160–176, Jan. 2010. doi: 10.1111/j.1365-2966.2009.15620.x.

C. Borys, S. Chapman, M. Halpern, and D. Scott. The Hubble Deep Field North SCUBA Super-map - I. Submillimetre maps, sources and number counts. MNRAS, 344(2):385–398, Sept. 2003. doi: 10.1046/j.1365-8711.2003.06818.x.

I. Cortzen, J. Garrett, G. Magdis, D. Rigopoulou, F. Valentino, M. Pereira-Santaella, F. Combes, A. Alonso-Herrero, S. Toft, E. Daddi, D. Elbaz, C. Gómez-Guijarro, M. Stockmann, J. Huang, and C. Kramer. PAHs as tracers of the molecular gas in star-forming galaxies. MNRAS, 482(2):1618–1633, Jan. 2019. doi: 10.1093/mnras/sty2777.

V. Desai, L. Armus, H. W. W. Spoon, V. Charmandaris, J. Bernard-Salas, B. R. Brandl, D. Farrah, B. T. Soifer, H. I. Teplitz, P. M. Ogle, D. Devost, S. J. U. Higdon, J. A. Marshall, and J. R. Houck. PAH Emission from Ultraluminous Infrared Galaxies. ApJ, 669(2):810–820, Nov. 2007. doi: 10.1086/522104.

H. Dole, R. Gispert, G. Lagache, J. L. Puget, F. R. Bouchet, C. Cesarsky, P. Ciliegi, D. L. Clements, M. Dennefeld, F. X. Désert, D. Elbaz, A. Franceschini, B. Guiderdoni, M. Harwit, D. Lemke, A. F. M. Moorwood, S. Oliver, W. T. Reach, M. Rowan-Robinson, and M. Stickel. FIRBACK: III. Catalog, source counts, and cosmological implications of the 170 mu m ISO. A&A, 372:364–376, June 2001. doi: 10.1051/0004-6361:20010449.

A. Efstathiou, D. Farrah, J. Afonso, D. L. Clements, E. González-Alfonso, M. Lacy, S. Oliver, V. Papadopoulou Lesta, C. Pearson, D. Rigopoulou, M. Rowan-Robinson, H. W. W. Spoon, A. Verma, and L. Wang. A new look at local ultraluminous infrared galaxies: the atlas and radiative transfer models of their complex physics. MNRAS, 512(4):5183–5213, June 2022. doi: 10.1093/mnras/stab3642.

D. Farrah, V. Lebouteiller, H. W. W. Spoon, J. Bernard-Salas, C. Pearson, D. Rigopoulou, H. A. Smith, E. González-Alfonso, D. L. Clements, A. Efstathiou, D. Cormier, J. Afonso, S. M. Petty, K. Harris, P. Hurley, C. Borys, A. Verma, A. Cooray, and V. Salvatelli. Far-infrared Fine-structure Line Diagnostics of Ultraluminous Infrared Galaxies. ApJ, 776(1):38, Oct. 2013. doi: 10.1088/0004-637X/776/1/38.

T. Goto, S. Arnouts, H. Inami, H. Matsuhara, C. Pearson, T. T. Takeuchi, E. Le Floc'h, T. Takagi, T. Wada, T. Nakagawa, S. Oyabu, D. Ishihara, H. Mok Lee, W.-S. Jeong, C. Yamauchi, S. Serjeant, C. Sedgwick, and E. Treister. Luminosity functions of local infrared galaxies with AKARI: implications for the cosmic star formation history and AGN evolution. MNRAS, 410(1):573–584, Jan. 2011. doi: 10.1111/j.1365-2966.2010.17466.x.

C. R. Harris, K. J. Millman, S. J. van der Walt, R. Gommers, P. Virtanen, D. Cournapeau, E. Wieser, J. Taylor, S. Berg, N. J. Smith, R. Kern, M. Picus, S. Hoyer, M. H. van Kerkwijk, M. Brett, A. Haldane, J. F. del Río, M. Wiebe, P. Peterson, P. Gérard-Marchant, K. Sheppard, T. Reddy, W. Weckesser, H. Abbasi, C. Gohlke, and T. E. Oliphant. Array programming with NumPy. *Nature*, 585(7825):357–362, Sept. 2020. doi: 10.1038/s41586-020-2649-2. URL `https://doi.org/10.1038/s41586-020-2649-2`.

J. D. Hunter. Matplotlib: A 2d graphics environment. *Computing in Science & Engineering*, 9(3):90–95, 2007. doi: 10.1109/MCSE.2007.55.

E. Jones, T. Oliphant, P. Peterson, et al. SciPy: Open source scientific tools for Python, 2001–. URL `http://www.scipy.org/`.

C. J. Lonsdale, D. Farrah, and H. E. Smith. Ultraluminous Infrared Galaxies. In J. W. Mason, editor, *Astrophysics Update 2*, page 285. 2006. doi: 10.1007/3-540-30313-8_9.

P. Madau and M. Dickinson. Cosmic Star-Formation History. ARA&A, 52:415–486, Aug. 2014. doi: 10.1146/annurev-astro-081811-125615.

A. Maragkoudakis, N. Ivkovich, E. Peeters, D. J. Stock, D. Hemachandra, and A. G. G. M. Tielens. PAHs

and star formation in the H II regions of nearby galaxies M83 and M33. MNRAS, 481(4):5370–5393, Dec. 2018. doi: 10.1093/mnras/sty2658.

A. M. J. Mortier, S. Serjeant, J. S. Dunlop, S. E. Scott, P. Ade, D. Alexander, O. Almaini, I. Aretxaga, C. Baugh, A. J. Benson, P. N. Best, A. Blain, J. Bock, C. Borys, A. Bressan, C. Carilli, E. L. Chapin, S. Chapman, D. L. Clements, K. Coppin, M. Crawford, M. Devlin, S. Dicker, L. Dunne, S. A. Eales, A. C. Edge, D. Farrah, M. Fox, C. Frenk, E. Gaztañaga, W. K. Gear, E. Gonzales-Solares, G. L. Granato, T. R. Greve, J. A. Grimes, J. Gundersen, M. Halpern, P. Hargrave, D. H. Hughes, R. J. Ivison, M. J. Jarvis, T. Jenness, R. Jimenez, E. van Kampen, A. King, C. Lacey, A. Lawrence, K. Lepage, R. G. Mann, G. Marsden, P. Mauskopf, B. Netterfield, S. Oliver, L. Olmi, M. J. Page, J. A. Peacock, C. P. Pearson, W. J. Percival, A. Pope, R. S. Priddey, S. Rawlings, N. Roche, M. Rowan-Robinson, D. Scott, K. Sekiguchi, M. Seigar, L. Silva, C. Simpson, I. Smail, J. A. Stevens, T. Takagi, G. Tucker, C. Vlahakis, I. Waddington, J. Wagg, M. Watson, C. Willott, and M. Vaccari. The SCUBA Half-Degree Extragalactic Survey - I. Survey motivation, design and data processing. MNRAS, 363(2):563–580, Oct. 2005. doi: 10.1111/j.1365-2966.2005.09460.x.

M. Rowan-Robinson, R. G. Mann, S. J. Oliver, A. Efstathiou, N. Eaton, P. Goldschmidt, B. Mobasher, S. B. G. Serjeant, T. J. Sumner, L. Danese, D. Elbaz, A. Franceschini, E. Egami, M. Kontizas, A. Lawrence, R. McMahon, H. U. Norgaard-Nielsen, I. Perez-Fournon, and J. I. Gonzalez-Serrano. Observations of the Hubble Deep Field with the Infrared Space Observatory - V. Spectral energy distributions, starburst models and star formation history. MNRAS, 289(2):490–496, Aug. 1997. doi: 10.1093/mnras/289.2.490.

H. V. Shipley, C. Papovich, G. H. Rieke, M. J. I. Brown, and J. Moustakas. A New Star Formation Rate Calibration from Polycyclic Aromatic Hydrocarbon Emission Features and Application to High-redshift Galaxies. ApJ, 818(1):60, Feb. 2016. doi: 10.3847/0004-637X/818/1/60.

B. T. Soifer and G. Neugebauer. The Properties of Infrared Galaxies in the Local Universe. AJ, 101:354, Feb. 1991. doi: 10.1086/115691.

M. Vaccari, L. Marchetti, A. Franceschini, B. Altieri, A. Amblard, V. Arumugam, R. Auld, H. Aussel, T. Babbedge, A. Blain, J. Bock, A. Boselli, V. Buat, D. Burgarella, N. Castro-Rodríguez, A. Cava, P. Chanial, D. L. Clements, A. Conley, L. Conversi, A. Cooray, C. D. Dowell, E. Dwek, S. Dye, S. Eales, D. Elbaz, D. Farrah, M. Fox, W. Gear, J. Glenn, E. A. González Solares, M. Griffin, M. Halpern, E. Hatziminaoglou, J. Huang, E. Ibar, K. Isaak, R. J. Ivison, G. Lagache, L. Levenson, N. Lu, S. Madden, B. Maffei, G. Mainetti, A. M. J. Mortier, H. T. Nguyen, B. O'Halloran, S. J. Oliver, A. Omont, M. J. Page, P. Panuzzo, A. Papageorgiou, C. P. Pearson, I. Pérez-Fournon, M. Pohlen, J. I. Rawlings, G. Raymond, D. Rigopoulou, D. Rizzo, G. Rodighiero, I. G. Roseboom, M. Rowan-Robinson, M. Sánchez Portal, B. Schulz, D. Scott, N. Seymour, D. L. Shupe, A. J. Smith, J. A. Stevens, M. Symeonidis, M. Trichas, K. E. Tugwell, E. Valiante, I. Valtchanov, L. Vigroux, L. Wang, R. Ward, G. Wright, C. K. Xu, and M. Zemcov. The HerMES SPIRE submillimeter local luminosity function. A&A, 518:L20, July 2010. doi: 10.1051/0004-6361/201014694.

Wes McKinney. Data Structures for Statistical Computing in Python. In Stéfan van der Walt and Jarrod Millman, editors, *Proceedings of the 9th Python in Science Conference*, pages 56 – 61, 2010. doi: 10.25080/Majora-92bf1922-00a.